



## Article

# The Only Chemoreceptor Encoded by *che* Operon Affects the Chemotactic Response of *Agrobacterium* to Various Chemoeffectors

Jingyang Ye, Miaomiao Gao, Qingxuan Zhou, Hao Wang, Nan Xu and Minliang Guo \*

College of Bioscience and Biotechnology, Yangzhou University, Yangzhou 225009, China; DX120170118@yzu.edu.cn (J.Y.); miaomiaogao1@163.com (M.G.); m18362821722@163.com (Q.Z.); wanghao@yzu.edu.cn (H.W.); nanxu@yzu.edu.cn (N.X.)

\* Correspondence: guoml@yzu.edu.cn; Tel.: +86-0514-87962283; Fax: +86-0514-87991747

**Abstract:** Chemoreceptor (also called methyl-accepting chemotaxis protein, MCP) is the leading signal protein in the chemotaxis signaling pathway. MCP senses and binds chemoeffectors, specifically, and transmits the sensed signal to downstream proteins of the chemotaxis signaling system. The genome of *Agrobacterium fabrum* (previously, *tumefaciens*) C58 predicts that a total of 20 genes can encode MCP, but only the MCP-encoding gene *atu0514* is located inside the *che* operon. Hence, the identification of the exact function of *atu0514*-encoding chemoreceptor (here, named as MCP<sub>514</sub>) will be very important for us to understand more deeply the chemotaxis signal transduction mechanism of *A. fabrum*. The deletion of *atu0514* significantly decreased the chemotactic migration of *A. fabrum* in a swim plate. The test of *atu0514*-deletion mutant ( $\Delta 514$ ) chemotaxis toward single chemicals showed that the deficiency of MCP<sub>514</sub> significantly weakened the chemotactic response of *A. fabrum* to four various chemicals, sucrose, valine, citric acid and acetosyringone (AS), but did not completely abolish the chemotactic response. MCP<sub>514</sub> was localized at cell poles although it lacks a transmembrane (TM) region and is predicted to be a cytoplasmic chemoreceptor. The replacement of residue Phe328 showed that the helical structure in the hairpin subdomain of MCP<sub>514</sub> is a direct determinant for the cellular localization of MCP<sub>514</sub>. Single respective replacements of key residues indicated that residues Asn336 and Val353 play a key role in maintaining the chemotactic function of MCP<sub>514</sub>.

**Keywords:** *Agrobacterium fabrum*; chemotaxis; chemoreceptor; cellular localization; methyl-accepting chemotaxis protein; chemoeffector



**Citation:** Ye, J.; Gao, M.; Zhou, Q.; Wang, H.; Xu, N.; Guo, M. The Only Chemoreceptor Encoded by *che* Operon Affects the Chemotactic Response of *Agrobacterium* to Various Chemoeffectors. *Microorganisms* **2021**, *9*, 1923. <https://doi.org/10.3390/microorganisms9091923>

Academic Editor: Toni A. Chapman

Received: 12 August 2021

Accepted: 7 September 2021

Published: 10 September 2021

**Publisher's Note:** MDPI stays neutral with regard to jurisdictional claims in published maps and institutional affiliations.



**Copyright:** © 2021 by the authors. Licensee MDPI, Basel, Switzerland. This article is an open access article distributed under the terms and conditions of the Creative Commons Attribution (CC BY) license (<https://creativecommons.org/licenses/by/4.0/>).

## 1. Introduction

Chemotaxis is an adaptive behavior of motile bacteria moving along the concentration gradient of chemoeffectors towards an optimal environment [1,2]. This adaptive behavior is regulated by a two-component system composed of histidine kinase CheA and chemotaxis response regulator protein CheY [3,4]. When a chemical attractant exists in the environment, methyl-accepting chemotaxis protein (MCP) can bind the attractant, and the ligand binding will change the conformation of MCP; then, through a coupling protein CheW, the kinase activity of CheA will be suppressed. The suppression of CheA activity will delay the transfer of the phosphoryl group to the response regulator protein CheY, resulting in the decrease in phosphorylated CheY [5,6]. The absence of phosphorylated CheY makes less change of the rotational direction of flagella and thus keeps bacteria swimming to the attractant. On the contrary, when the concentration of attractant goes down (or repellent goes up), MCP activates the kinase activity of CheA. Self-phosphorylated CheA passes the phosphoryl groups to CheY. Phosphorylated CheY will bind to the flagellar motor and change the rotational direction of flagella frequently, which causes cell tumbling and changes direction away from the adverse environment [7,8].

Many bacteria possess chemotactic behavior for a large number of chemicals, such as different nitrogen or carbon nutrient substances, different environmental pollutants, or different signal chemicals released by their ecological partners [9–13]. To sense the vast

chemoeffectors, bacteria must evolve an enormous number of different chemoreceptors. A typical chemoreceptor contains an N-terminal periplasmic ligand binding domain (LBD), a transmembrane (TM) helical region, a HAMP (existing in histidine kinases, adenylate cyclases, methyl-accepting chemotaxis proteins, and phosphatases) domain, and a C-terminal cytoplasmic signaling domain (SD), comprising a methyl-accepting (MA) subdomain, a flexible bundle (FB) subdomain, and a hairpin (HP) subdomain (Figure 1A) [7,14,15]. The hairpin subdomain interacts with the coupling protein CheW and the sensor kinase CheA. Chemoreceptors use LBD to recognize chemoeffectors. In order to recognize different chemicals, chemoreceptors have evolved many different types of LBDs [9]. According to the LBD and membrane topology, chemoreceptors can be divided into four classes, of which class IV is cytoplasmic (soluble) chemoreceptors and the rest are transmembrane chemoreceptors. Based on the length from the N-terminus to the MA domain, cytoplasmic chemoreceptors can be divided into two subclasses of IVa and IVb. The N-terminal domain of IVa has at least 108 amino acids, while the N-terminal domain of IVb is shorter than 108 amino acids [16,17]. Among 8384 chemoreceptors defined by the MA subdomain in the complete genome of the SMART database [18], 14% of the chemoreceptors are cytoplasmic chemoreceptors. The ligand-binding motif is generally predicted at the N-terminal of IVa subclass chemoreceptors. Based on the statistical analysis of 1129 chemoreceptors with LBD in the SMART database, 47% of LBD is PAS domain, such as AerC in *A. brasilense* [19]; CZB domain found in *Helicobacter pylori* TlpD [20], is the second most common LBD, accounting for 8% of all IVa chemoreceptors; protoglobin [21] is the third most common LBD, accounting for 7% of all IVa chemoreceptors; the remaining domains account for less than 1% [22].

*Agrobacterium fabrum* is a Gram-negative bacterium and induces crown gall tumor disease in most dicotyledonous plants by genetically transforming the host [23,24]. In the natural environment, *A. fabrum* is usually distributed around the rhizosphere of a plant, and chemotaxis is an important first process of its interaction with the host. It has two kinds of lifestyles; one is to survive in the soil environment independently and the other is symbiotic with the plant as a pathogen [25–27]. Only when it recognizes and senses the sugars, acidic pH or phenols released by the host can *A. fabrum* begin the infecting process by chemotaxis toward the wound site of the host [28]. In the late 1980s, chemotaxis of *A. fabrum* was preliminarily studied, proving that it can respond to sugars, amino acids and phenols released by the injured plant tissues [29–31], but the specific chemotaxis mechanism has been rarely studied [32]. The genome sequence of *A. fabrum* C58 predicts that it has only one chemotaxis gene cluster (*che* cluster). The gene organization of this gene cluster is shown in Figure 1B. This gene cluster contains the genes encoding most components of the chemotaxis system. Spaces between the adjacent genes are very short and some adjacent genes even share a few nucleotides. All the genes in this cluster are predicted to be controlled by the same upstream promoter and thus located on the same operon [12,33]. In addition to the *atu0514* gene, the only gene annotated to encode MCP in this *che* operon, *A. fabrum* carries an additional 19 MCP-encoding genes, including 1 on the Ti plasmid, 1 on the At plasmid, 5 on the linear chromosome, and the remaining 12 on the circular chromosome [33]. The number of MCPs in *A. fabrum* C58 indicates its complex chemotaxis signal and strong environmental adaptability [34].

The *A. fabrum* *atu0514* gene, located on the circular chromosome, is the only MCP-encoding gene in the *che* operon [12]. Unlike all other MCPs, MCP<sub>514</sub> is co-expressed with all other core chemotaxis components. Therefore, it may be the most important chemoreceptor, and characterizing its function is very helpful for us to further understand the chemotaxis signal transduction mechanism of *A. fabrum*. In this study, we firstly constructed the *atu0514*-deletion mutant  $\Delta$ 514 and the complemented strain  $\Delta$ 514-C and tested the effect of *atu0514*-deficiency on the chemotactic response of *A. fabrum* C58. We also identified the key residues that affect the cellular localization and function of MCP<sub>514</sub>.

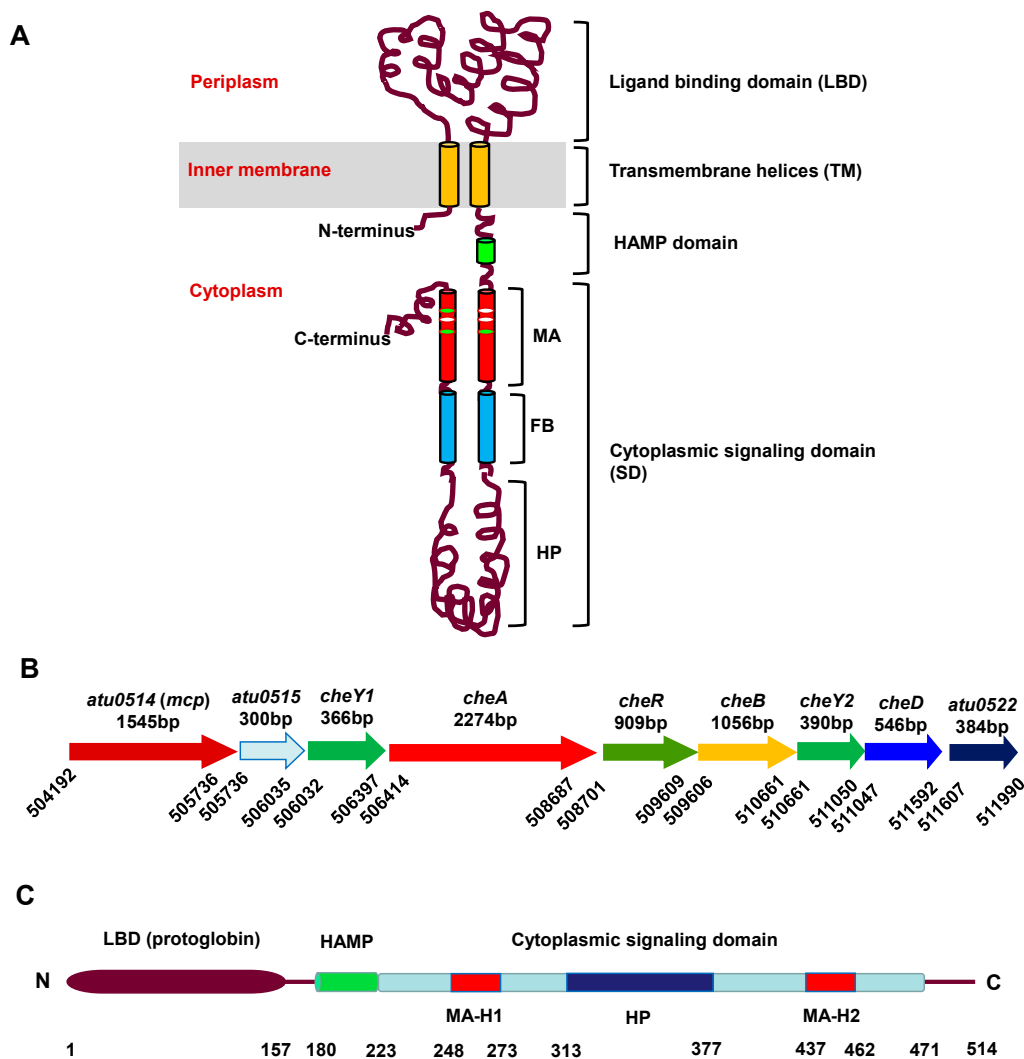


**Figure 1.** Topological structure of a typical MCP, gene organization of a *A. fabrum che* gene cluster and domain organization of MCP<sub>514</sub>. (A) Architectural model of a typical MCP. Cylinders represent  $\alpha$ -helices. MA: methyl-accepting (or sensory adaptation) subdomain; FB: flexible bundle subdomain; HP: hairpin subdomain. (B) Gene organization of *A. fabrum che* gene cluster. Arrows represent genes. Above the arrows are the names and lengths of the genes. Numbers under the arrows indicate the nucleotide position of the gene border. (C) Predicted domain organization of MCP<sub>514</sub>. MA-H1:  $\alpha$ -helix 1 of MA subdomain; MA-H2:  $\alpha$ -helix 2 of MA subdomain; numbers under the domains indicate the amino acid position of the domain border.

## 2. Materials and Methods

### 2.1. Primers, Plasmids, Bacterial Strains and Growth Conditions

The primers, plasmids and bacterial strains used in this study are listed in Supplementary Tables S1 and S2. Lysogeny broth (LB) liquid or agar medium was used to grow *E. coli* at 37 °C [35]. *A. fabrum* was grown in MG/L or AB-sucrose liquid or agar medium at 28 °C [36,37]. Concentrations of ampicillin and kanamycin used for *E. coli* were 100 and 50  $\mu\text{g}/\text{mL}$ , respectively. Concentrations of kanamycin and carbenicillin for *A. fabrum* were 100  $\mu\text{g}/\text{mL}$ .

### 2.2. DNA Manipulations

DNA manipulations followed the standard molecular protocols [35]. Plasmid isolation was performed with the TIANprep Mini Plasmids Kit (TIANGEN BIOTECH Corporation, Beijing, China). PCR products obtained by Veriti 96-well cycler (Thermo Fisher Scientific Inc., Waltham, MA USA) and DNA fragments were purified from agarose gels by using

the TaKaRa MiniBEST Agarose Gel DNA Extraction Kit (TaKaRa Corporation, Dalian, China). Plasmids were transferred into *E. coli* competent cells by heat-shock [35] and into *A. fabrum* by the Eppendorf electroporation instrument Eporator<sup>®</sup> (Eppendorf AG, Hamburg, Germany) [36].

### 2.3. Mutagenesis and Complementation of *Atu0514*

Based on the principle of homologous recombination, we used the pEX18Km-derived gene replacement plasmids to construct the corresponding gene deletion mutants [38,39]. Plasmid pEX18Km carries both a positive selection marker (kanamycin resistance,  $K_m^R$ ) and counterselectable marker (suicide gene *sacB*) and cannot be replicated in *A. fabrum*. The positive selection marker allowed to select the transformants, in which the whole plasmid was integrated into the genome by the first homologous recombination. The counterselectable marker allowed to counterselect the transformants, in which both the target DNA fragment and the undesirable plasmid backbone were deleted from the genome by the second homologous recombination. The combined utilization of selectable and counterselectable markers can precisely generate an unmarked mutant without any undesirable DNA fragment (Figure S1A). *A. fabrum* wild type C58 was used to construct the *atu0514*-deletion mutant  $\Delta 514$ . *A. fabrum cheW<sub>1</sub>-cheW<sub>2</sub>* double-deletion mutant  $\Delta w$  [40] was used to construct *atu0514-cheW<sub>1</sub>-cheW<sub>2</sub>* triple-deletion mutant  $\Delta 514\Delta w$ . The desirable mutant was screened using PCR (Figure S1B) and verified by sequencing. The DNA fragment encoding amino acids 14–453 of MCP<sub>514</sub> was precisely deleted in both  $\Delta 514$  and  $\Delta 514\Delta w$  mutants (Figure S1C). The complementation of MCP<sub>514</sub> in the *atu0514*-deletion mutant was fulfilled by the introduction of plasmid expressing MCP<sub>514</sub> (or its variants). Gene fusions with the *egfp* as well as deletion constructs were created by overlap extension PCR, as described by Higuchi [41]. These *egfp*-fused genes were cloned into the modified vector pUCA19 to generate the plasmids expressing eGFP-fused proteins. When these eGFP-fused proteins were expressed in *A. fabrum* cells, the cellular localizations of these eGFP-fused proteins could be observed by using Zeiss confocal microscope LSM 880 NLO (Carl Zeiss AG, Oberkochen, Germany).

### 2.4. Chemotaxis Assays

The procedure of capillary assay was followed as described by Adler in 1973 [42], with minor modifications. *A. fabrum* cells were harvested from mid-log-phase culture by centrifugation at 4000 rpm for 3 min at room temperature (25 °C) and suspended in chemotaxis buffer (0.1 mmol/L EDTA, 10 mmol/L KH<sub>2</sub>PO<sub>4</sub>, pH 7.0) to an OD<sub>600nm</sub> of 0.1. *A. fabrum* cell suspension (300  $\mu$ L) was used to make a bacterial pond. The capillary tube was sealed at one end and filled with attractant at peak concentration dissolved in the chemotaxis buffer. The open end of the capillary tube was inserted into the bacterial pond and incubated for 1 h at room temperature (25 °C), then, the solution in the capillary tube was expelled and completely transferred into 1 mL of AB-sucrose medium. Dilutions were plated in duplicate on MG/L plates and incubated for 2 days at 28 °C. The colonies in the plates were counted and represented the number of cells attracted to the capillary tube.

The procedure of swim agar plate assay was followed that described by Merritt [43], with minor modifications. The tested strains were inoculated in AB-sucrose liquid medium and grown to the middle log phase, and then, the OD<sub>600nm</sub> was adjusted to 0.6 by using AB-sucrose liquid medium. A total of 3  $\mu$ L of bacterial suspension was dropped onto an AB-sucrose swim plate containing 0.2% agar, and 5 replicates were set. After incubation at 28 °C for 36–48 h, the diameter of the bacterial colony circle was measured, and the data were statistically analyzed.

### 2.5. Bacterial Two-Hybrid Analyses

The bacterial two-hybrid system from the Stratagene<sup>®</sup> (Agilent Technologies Inc., Santa Clara, CA, USA) was used for testing protein–protein interactions. All the operations were conducted according to the manual. The open read frame (ORF) of *atu0514* was

inserted into the bait plasmid pBT to express  $\lambda$ CI-MCP<sub>514</sub> (bait) fusion protein. ORFs of *cheW*<sub>1</sub> and *cheW*<sub>2</sub> were inserted to the target plasmid pTRG to express CheW<sub>1</sub> (target)–RNAP and CheW<sub>2</sub> (target)–RNAP fusion proteins, respectively. The interaction between bait (MCP<sub>514</sub>) and target (CheW<sub>1</sub> or CheW<sub>2</sub>) will take  $\lambda$ CI and RNAP together to induce the expression of  $\beta$ -galactosidase, and thus, the bacterial colonies growing on plates containing 80  $\mu$ g/mL X-gal will be blue. Otherwise, the bacterial colonies will be of normal color. Galactosidase activity was determined by the method of Miller [44].

### 2.6. Fluorescence Microscopy

For microscopy observation, agrobacterial cells from the mid-log-phase cultures were added to the center of the slides. A coverslip was placed on top of the culture droplet. The edges of the coverslip were sealed with acrylic polymer to prevent drying. *A. fabrum* cells were visualized by a Zeiss LSM 880 NLO system (Carl Zeiss AG, Oberkochen, Germany) using an Ar laser (excitation wavelength of 488 nm and emission wavelength of 500 to 550 nm) and a  $\times 100$  oil immersion objective. The images were analyzed and edited using ZEN lite (Blue edition), version 3.2 (Carl Zeiss AG, Oberkochen, Germany).

### 2.7. Statistical Analysis

The quantitative data shown in this study were the means with the standard deviations (SDs), which were derived from at least three independent experiments conducted in triplicate. Differences among bacterial strains were compared using one-way analysis of variance (ANOVA), followed by the Tukey test for multiple comparisons. The statistical analysis was conducted using Microsoft Office Excel's data analysis tool (2019 version) (Microsoft Corporation, Redmond, WA, USA).

## 3. Results

### 3.1. MCP<sub>514</sub> Is a Cytoplasmic Chemoreceptor, but Localized at Cell Poles

By SMART analysis, MCP<sub>514</sub> has a total of 514 amino acids and carries three conserved domains, protoglobin domain, HAMP domain and cytoplasmic signal domain (SD), in the order from N-terminal to C-terminal (Figure 1C). The protoglobin domain of MCP<sub>514</sub> shares 13.51% sequence identity with the LBD of HEMAT, a cytoplasmic chemoreceptor from *B. subtilis* [21], through the SWISS-Model homology search. According to Alexandre's heptapeptide classification, cytoplasmic signal domain (SD) belongs to the 36H family [45]. The two best-studied MCPs of the 36H family are Tsr and Tar proteins of *E. coli*. Further analysis on the secondary structure of MCP<sub>514</sub> by SOSUI [46] and SPLIT [47] shows that MCP<sub>514</sub> does not contain the hydrophobic domain, indicating that MCP<sub>514</sub> does not possess a transmembrane (TM) region and belongs to an IVa cytoplasmic chemoreceptor.

Transmembrane chemoreceptors are mainly localized at cell poles, but the cytoplasmic chemoreceptors have a wider cellular localization mode, ranging from co-localization with transmembrane chemoreceptor arrays to a diffuse cytoplasmic distribution [48]. The localization of some cytoplasmic chemoreceptors is associated with the physiology and life cycle of bacteria [22]. According to previous classification [9], MCP<sub>514</sub> should be classified into the category of the cytoplasmic chemoreceptor due to the lack of a transmembrane region, but we do not know the cellular localization of MCP<sub>514</sub>. To observe the cellular localization of MCP<sub>514</sub>, the enhanced green fluorescent protein (eGFP) was fused to the N-terminus of MCP<sub>514</sub> because only the N-terminally GFP-tagged MCP<sub>514</sub> was functional [49]. This eGFP-MCP<sub>514</sub> fusion protein was expressed in the MCP<sub>514</sub>-deficient strain  $\Delta$ 514. Figure 2A showed that the eGFP-MCP<sub>514</sub> fusion protein is localized at the poles of the *A. fabrum* cell. However, the eGFP-MCP<sub>514</sub> fusion protein is distributed in the whole cell of *E. coli* (Figure 2B), verifying that MCP<sub>514</sub> lacks a transmembrane domain. These data also imply that the polar localization of MCP<sub>514</sub> in *A. fabrum* cell requires the assistance of other *A. fabrum* proteins.

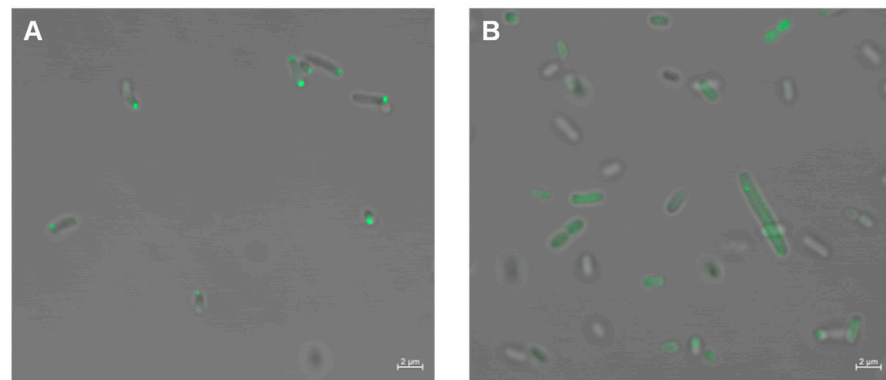


**Figure 2.** Cellular localization of MCP<sub>514</sub>. Plasmid expressing the eGFP–MCP<sub>514</sub> fusion protein was introduced into *A. fabrum* MCP<sub>514</sub>-deficient mutant Δ514 (A) and *E. coli* strain DH5α (B), respectively. Bacterial cells were grown to middle-log phase and observed by using confocal laser-scanning microscopy.

### 3.2. MCP<sub>514</sub> Significantly Affects the Chemotactic Response of *Agrobacterium Fabrum*

Since MCP<sub>514</sub> is localized at cell poles, we next try to test the effect of MCP<sub>514</sub> on the chemotactic response of *A. fabrum*. When bacterium grows on the swim agar plate, the utilization of nutrient substances by bacterium will result in a nutrient concentration gradient. Bacterium with chemotaxis will move outward along the nutrient concentration gradient and grow a big colony. Consequently, the overall chemotactic response to nutrient substances can be characterized by measuring the colony size in the swim agar plate [10]. *A. fabrum* has only one CheA, and CheA is the key component of a chemotaxis system. The deletion of the *cheA* gene will completely abolish the chemotactic response of *A. fabrum*, and thus, the CheA-deficient mutant Δ*a* was used as a control of chemotaxis deficiency [40]. As shown in Figure 3, the deficiency of MCP<sub>514</sub> significantly attenuates the overall chemotactic response of *A. fabrum* to nutrient substances. The complementation of MCP<sub>514</sub> by the introduction of MCP<sub>514</sub>-expressing plasmid can fully restore the chemotactic response of the MCP<sub>514</sub>-deficient mutant to the level of the wildtype, confirming the role of MCP<sub>514</sub> in the chemotactic response. These results also provided evidence that the deletion of *atu0514* did not have a polar effect on the rest of the *che* operon. Previous research showed that *A. fabrum* has chemotaxis toward sugars, amino acids, organic acids and phenols [29,30]. The traditional capillary assay is an effective method for quantifying the chemotaxis ability of bacteria [42]. The chemotactic responses of wildtype C58, mutant Δ514 and complemented strain Δ514-C to four various chemicals (1 μmol/L sucrose, 1 mmol/L valine, 1 mmol/L citric acid and 0.1 μmol/L acetosyringone (AS)) were measured by using the traditional capillary method. As shown in Figure 4, the deletion of *atu0514* significantly weakens the chemotaxis of *A. fabrum* toward these four different types of chemicals. However, the chemotaxis of strain Δ514 toward these chemicals does not completely disappear, indicating that MCP<sub>514</sub> is not the receptor directly recognizing these substances but affects the chemotaxis efficiency in other ways.

### 3.3. Both CheW<sub>1</sub> and CheW<sub>2</sub> Interact with MCP<sub>514</sub> but Do Not Affect the Cellular Localization of MCP<sub>514</sub>

It is known that CheW couples CheA to chemoreceptors and forms stable ternary signaling complexes with chemoreceptors and CheA [3]. To confirm the role of MCP<sub>514</sub> in the chemotaxis signal transduction pathway of *A. fabrum*, the bacterial two-hybrid system was used to test the interaction between MCP<sub>514</sub> and two CheWs. As shown in Figure 5A, the colors of the colonies representing MCP<sub>514</sub>/CheW<sub>1</sub> and MCP<sub>514</sub>/CheW<sub>2</sub> interaction are bluer than that of the negative control. The quantification of β-galactosidase activity also showed that the β-galactosidase activities of the colonies expressing these two tested protein pairs (MCP<sub>514</sub>/CheW<sub>1</sub> and MCP<sub>514</sub>/CheW<sub>2</sub>) are significantly higher than that of

the negative control (Figure 5B). This indicates that MCP<sub>514</sub> protein interacted with both CheW<sub>1</sub> and CheW<sub>2</sub> proteins.

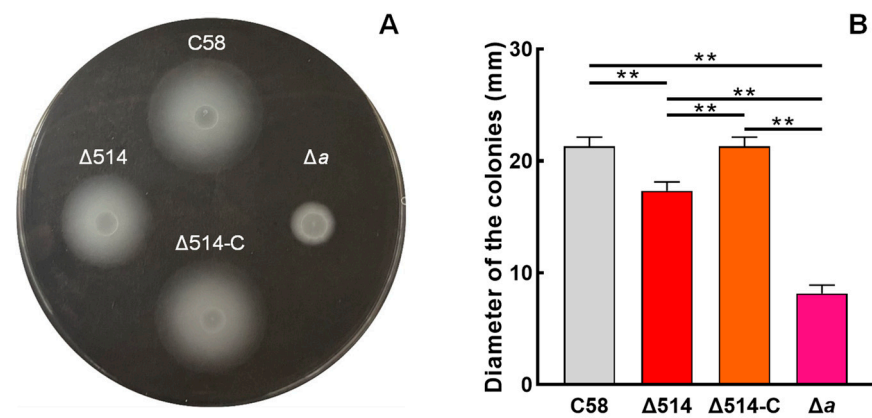


**Figure 3.** Effect of MCP<sub>514</sub> deficiency on the chemotactic response of *A. fabrum*. The tested *A. fabrum* strains were grown to middle-log phase. Bacterial cells were collected and resuspended to the same OD<sub>600nm</sub> (0.6). Equal amounts of cells from these cell suspensions were inoculated on the swim plates. The plates were incubated at 28 °C for 2 days. (A) Typical colonies of these tested *A. fabrum* strains. (B) The swim-ring diameters of these tested *A. fabrum* strains on the swim plate. The data represent the means ± SDs from five independent experiments in triplicate. The bars paired with two asterisks “\*\*” represent that they are statistically different at *p* < 0.01 via the one-way ANOVA, followed by Tukey test. C58, *A. fabrum* wildtype C58; Δ514, MCP<sub>514</sub>-deficient mutant; Δ514-C, Δ514 mutant complemented with MCP<sub>514</sub> through plasmid; Δa, CheA-deficient mutant (a control of chemotaxis deficiency).

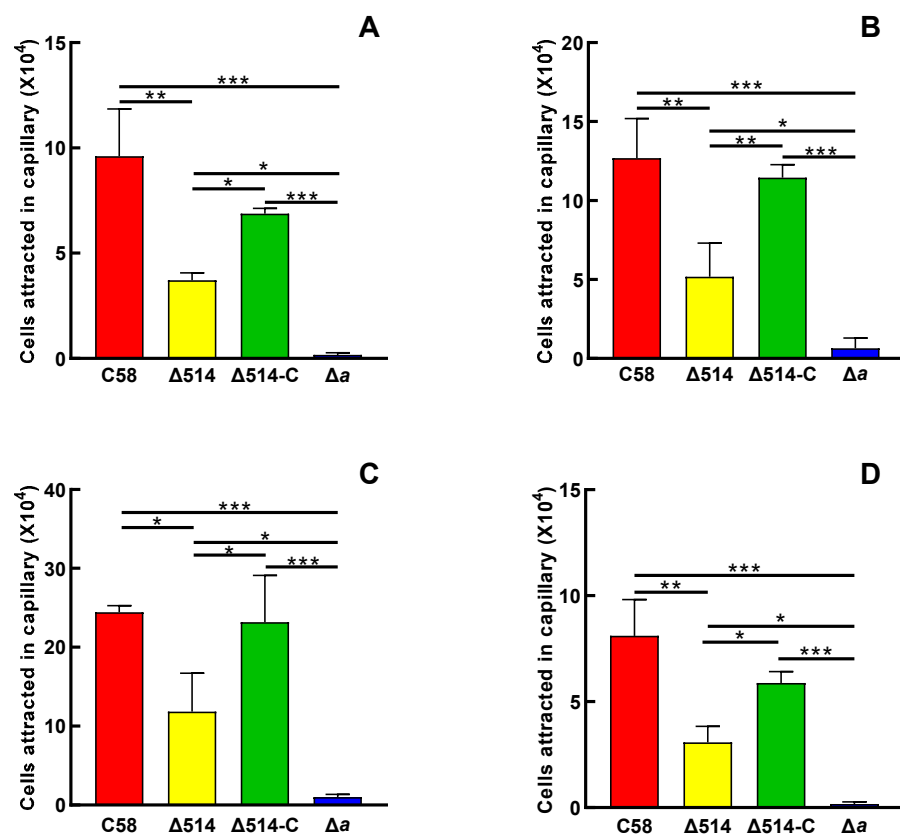


**Figure 4.** Effect of MCP<sub>514</sub> deficiency on the chemotactic responses of *A. fabrum* to sucrose (A), valine

(B), citric acid (C) and acetosyringone (D). *A. fabrum* cells in the middle-log phase were collected, washed and then adjusted to an  $OD_{600nm}$  of 0.1 with chemotaxis buffer. Capillary tubes containing chemotaxis buffer with  $10^{-6}$  mol/L sucrose,  $10^{-3}$  mol/L valine,  $10^{-3}$  mol/L citric acid, or  $10^{-7}$  mol/L acetosyringone were inserted into the cell suspensions for 1 h at room temperature (25 °C). Cells migrating to the capillary tube were counted by using colony count. The attracted cells are equal to the cells in the capillary tube with attractant minus the cells in the capillary tube without attractant. The data represent the means  $\pm$  SDs from three independent experiments with triplicate. The bars paired with “\*”, “\*\*” and “\*\*\*” marks represent that they are different in a statistical manner at  $p < 0.05$ , 0.01 and 0.001, respectively, via the one-way ANOVA, followed by Tukey test. The strain names in the horizontal axis are the same as in Figure 3.

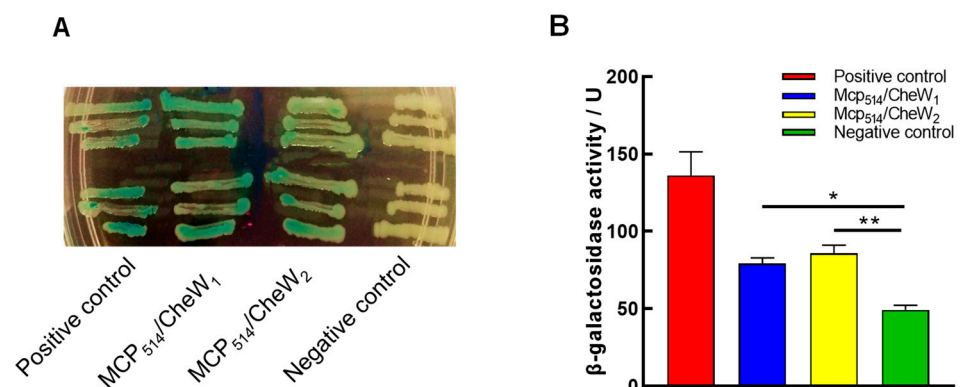


**Figure 5.** The interactions of MCP<sub>514</sub> with two CheWs of *A. fabrum*. The interaction between MCP<sub>514</sub> and CheW was tested by using a bacterial two-hybrid assay. All the operations followed the manual. The interaction between two tested proteins will induce the expression of β-galactosidase, and bacterial colonies will show blue color on the X-gal indicator plate. (A) Colony color on the X-gal indicator plate. (B) The activity of β-galactosidase reporter induced by the interacting proteins. Data are the means  $\pm$  SDs from three independent experiments with triplicate. The bars paired with “\*” and “\*\*” marks represent that they are different in a statistical manner at  $p < 0.05$  and 0.01, respectively via the one-way ANOVA, followed by Tukey test. Positive control, interaction between two known proteins (LGF2 and Gal11P) provided by the manufacturer; MCP<sub>514</sub>/CheW<sub>1</sub>, interaction between MCP<sub>514</sub> and CheW<sub>1</sub>; MCP<sub>514</sub>/CheW<sub>2</sub>, interaction between MCP<sub>514</sub> and CheW<sub>2</sub>; negative control, without any interacting proteins.

Both CheW<sub>1</sub> and CheW<sub>2</sub> interact with MCP<sub>514</sub> and most of the ternary MCP-CheW-CheA complexes are localized in the cell poles. However, MCP<sub>514</sub> lacks a transmembrane domain. It is unknown whether the cellular localization of MCP<sub>514</sub> is dependent on the ternary MCP-CheW-CheA complex. Therefore, we tested the effects of the CheW deficiency on the cellular localization of MCP<sub>514</sub>. To determine whether CheW affects the cellular localization of MCP<sub>514</sub>, a plasmid expressing eGFP-MCP<sub>514</sub> fusion protein was transferred into the *atu0514-cheW<sub>1</sub>-cheW<sub>2</sub>* triple deletion mutant  $\Delta 514\Delta w$ . Fluorescence observation showed that MCP<sub>514</sub> in the CheW-deficient strain is still localized at cell poles, indicating that CheW deficiency does not affect the polar localization of MCP<sub>514</sub> (Figure 6).

### 3.4. Helical Structure of Hairpin Subdomain Is Required for the Cellular Localization of MCP<sub>514</sub>

Due to the lack of a transmembrane domain in MCP<sub>514</sub> and the evidence that CheW deficiency does not affect the polar localization of MCP<sub>514</sub>, it is most likely that MCP<sub>514</sub> is localized in the cell poles via interacting with other MCPs. Results from *E. coli* MCPs showed that the hairpin subdomain of MCP is a coiled-coil of two antiparallel helices with a ‘U-turn’ and two hairpin subdomains form a supercoiled four-helical bundle, which makes MCP form homodimeric molecules [50]. The dimers of different MCPs can form mixed trimers of dimers via the interactions between their highly conserved helical bundle, and several residues play key roles in the formation of trimer (Figure S1) [51–53].

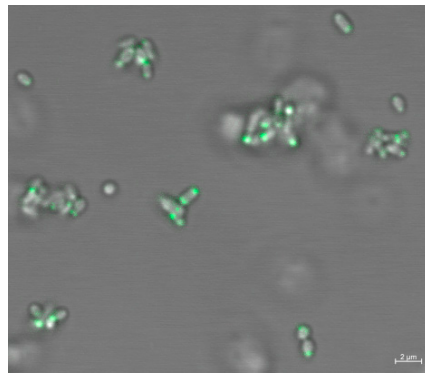


**Figure 6.** Cellular localization of MCP<sub>514</sub> in CheW-deficient *A. fabrum* mutant. Plasmid expressing eGFP-MCP<sub>514</sub> fusion protein was introduced into the *atu051–cheW<sub>1</sub>–cheW<sub>2</sub>* triple-deletion mutant  $\Delta 514\Delta w$ . Cells were grown to the middle-log phase and observed by using confocal laser-scanning microscopy.

To determine if the hairpin subdomain of MCP<sub>514</sub> affects the cellular localization of MCP<sub>514</sub>, key residue Phe328 in the hairpin subdomain was changed to Ala, Pro or Trp. These three single-residue-substituted MCP<sub>514</sub> variants were fused to eGFP, respectively. Fluorescence observation showed that the substitution of Phe328 for Pro causes the MCP<sub>514</sub> diffusion in the cytoplasm (Figure 7C), whereas the replacement of Phe328 by Ala or Trp does not affect the polar location of MCP<sub>514</sub> (Figure 7A,B). Proline is a constraint on the formation of helix. Replacement of Phe328 by Pro will destroy the helical structure of the hairpin subdomain. These results demonstrated that the helical structure of the hairpin subdomain is required for the cellular localization of MCP<sub>514</sub>.

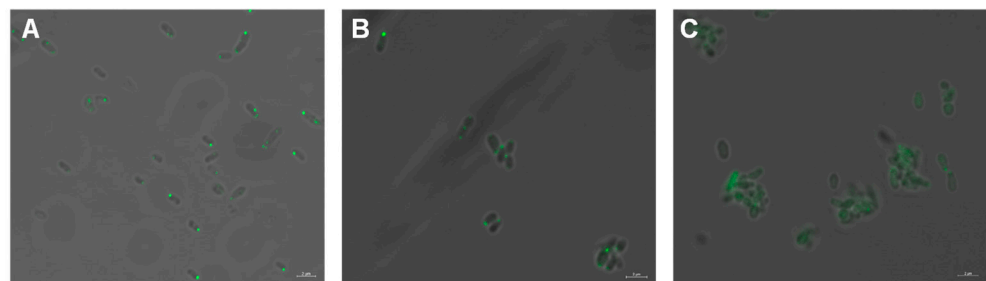


**Figure 7.** Effects of the substitution of key residue Phe328 on the cellular localization of MCP<sub>514</sub>. Key residue Phe328 in the hairpin subdomain of MCP<sub>514</sub> was replaced by Ala, Pro or Trp to generate three MCP<sub>514</sub> variants, MCP<sub>514</sub><sup>F328A</sup> (A), MCP<sub>514</sub><sup>F328W</sup> (B) and MCP<sub>514</sub><sup>F328P</sup> (C). Three MCP<sub>514</sub> variants were fused to eGFP and expressed as the eGFP-MCP<sub>514</sub> variant in the MCP<sub>514</sub>-deficient mutant  $\Delta 514$ , respectively. *A. fabrum* mutant  $\Delta 514$  cells expressing these eGFP-MCP<sub>514</sub> variant fusion proteins were grown to the middle-log phase and observed by using confocal laser-scanning microscopy.

### 3.5. Two Key Residues of Hairpin Subdomain Play a Key Role in Maintaining the Chemotactic Function of MCP<sub>514</sub>

The cellular localization of MCP<sub>514</sub> is dependent on the hairpin subdomain, which is involved in the interactions between different MCPs, as well as the interactions with the CheA and CheW [54]. The chemotactic signal is collaboratively transduced by the mixed MCP teams, and all signals from different MCPs will converge to CheA [51]. It is reasonable that residues involving in the interaction between MCPs may affect the chemotactic function of MCP<sub>514</sub>.

To further determine the key residues of MCP<sub>514</sub> that are involved in the trimer contact, we aligned the sequence of MCP<sub>514</sub> with the sequences of Tsr and Tar from *E. coli* [55] and chose Phe328, Asn336, Glu340, Arg343 and Val353 of MCP<sub>514</sub> as the target residues of the

site-directed mutation (Figure S2). Five residues were respectively replaced by alanine to generate five single residue-substituted MCP<sub>514</sub> variants. These MCP<sub>514</sub> variants were expressed in the MCP<sub>514</sub>-deficient mutant ( $\Delta 514$ ) by the introduction of the MCP<sub>514</sub> variant-expressing plasmid, respectively. Colonies of the MCP<sub>514</sub>-deficient mutant expressing various MCP<sub>514</sub> variants are shown in Figure 8A. The diameters of these tested strain colonies were used to quantify the effects of various MCP<sub>514</sub> variants on the chemotactic response of *A. fabrum* [43]. As shown in Figure 8, two single residue-substituted MCP<sub>514</sub> variants, MCP<sub>514</sub><sup>N336A</sup> and MCP<sub>514</sub><sup>V353A</sup>, are unable to restore the chemotactic response of the MCP<sub>514</sub>-deficient mutant to the level of the wildtype, demonstrating that residues Asn336 and Val353 play a key role in maintaining the chemotactic function of MCP<sub>514</sub>.

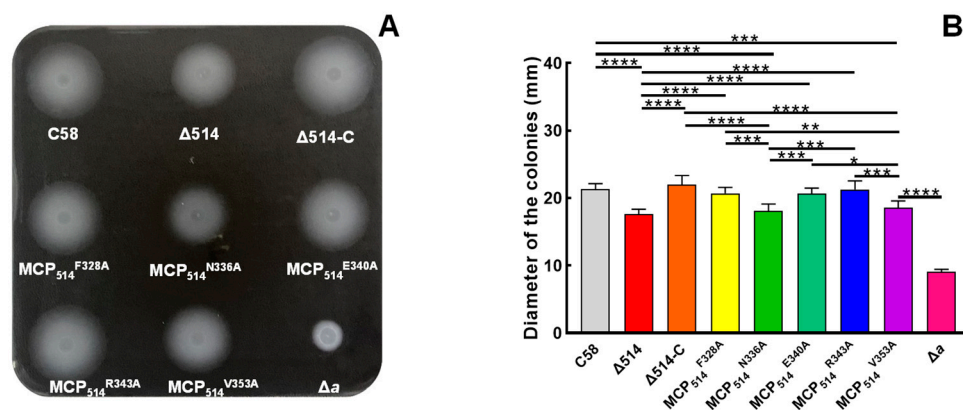


**Figure 8.** Effects of MCP<sub>514</sub> variants on the chemotactic response of *A. fabrum*. The test procedure was the same as described in Figure 3. (A) Typical colonies of these tested *A. fabrum* strains. (B) The swim-ring diameters of these tested *A. fabrum* strains on the swim plate. The data represent the means  $\pm$  SDs from five independent experiments in triplicate. The bars paired with “\*”, “\*\*”, “\*\*\*” and “\*\*\*\*” marks represent that they are different in a statistical manner at  $p < 0.05$ , 0.01, 0.001 and 0.0001, respectively, via the one-way ANOVA, followed by Tukey test. C58, *A. fabrum* wildtype C58 strain;  $\Delta 514$ , MCP<sub>514</sub> deficient mutant;  $\Delta 514$ -C,  $\Delta 514$  mutant complemented with native MCP<sub>514</sub>; MCP<sub>514</sub><sup>F328A</sup>, MCP<sub>514</sub><sup>N336A</sup>, MCP<sub>514</sub><sup>E340A</sup>, MCP<sub>514</sub><sup>R343A</sup> and MCP<sub>514</sub><sup>V353A</sup> represent  $\Delta 514$  mutant complemented with the corresponding single residue-substituted MCP<sub>514</sub> variants, respectively;  $\Delta a$ , CheA deficient mutant.

#### 4. Discussion

In natural environments, *A. fabrum* is usually distributed around the rhizosphere of a plant [24]. Chemotaxis is the important initial step for *A. fabrum* to infect the plant host [56]. Only when *A. fabrum* correctly recognizes and responds to the chemical signals released by the plant host can it contact the host plant, infect the host and start the tumorigenic processes [27,57–59]. MCPs are the first components of the chemotaxis system. The recognition of chemicals by these proteins is the initial stage of chemotaxis signaling transduction. Adaptive modification of the conserved glutamate domain of the MCP signal domain ensures that they are highly sensitive to different concentrations of chemoeffectors [60]. Although *A. fabrum* C58 contains 20 MCP-encoding genes, only one MCP-encoding gene (*atu0514*) is in the *che* operon [12]. It is rational that the MCP<sub>514</sub> encoded by the *atu0514* gene may play a unique role in the signaling transduction of chemotaxis.

Our results show that MCP<sub>514</sub> deficiency significantly affects not only the overall chemotactic response of *A. fabrum* to nutrient substances (Figure 3) but also the chemotaxis toward four various types of chemicals (Figure 4). The ligand binding domain (LBD) of MCP<sub>514</sub> is predicted to be a protoglobin, which cannot bind these four tested types of chemicals (Figure 1B). MCPs with different LBDs can form mixed trimers of dimers, and thousands of MCPs form a receptor cluster. The receptor cluster comprised of MCPs with different detection specificities collaboratively transduces the chemotactic signal in a team signaling model [51]. The effects of MCP<sub>514</sub> deficiency on the chemotaxis of *A. fabrum* toward four various types of chemicals demonstrate that MCP<sub>514</sub> is a very important

member of the chemoreceptor signaling team, and the absence of MCP<sub>514</sub> will affect the signaling efficiency of the whole chemoreceptor signaling team, explicating the reason of the *atu0514* gene locating the *che* operon.

Based on the sequenced genomes, 43% of archaeal and 14% of bacterial MCPs lack a transmembrane (TM) region. These TM-lacking MCPs are classified as cytoplasmic chemoreceptors. Unlike the transmembrane chemoreceptors, which are mainly located at the pole of the cell, cytoplasmic MCPs adopt more exotic locations [22]. Some cytoplasmic chemoreceptors are polarized at one end of the cell, such as, the HemAt of *B. subtilis* and the IcpA of *S. meliloti* [21,61]; other cytoplasmic chemoreceptors have both polar and diffuse states, for example, the AerC of *A. brasilense* was diffused in cytoplasm under an oxygen-rich environment but located in the cell polar under symbiotic nitrogen-fixing state, which helps cells adapt to hypoxic environments [19]. There are also some bacteria whose cytoplasmic chemoreceptors formed clusters in the cytoplasm, for example, the TlpC and TlpT of *R. sphaeroides* are located in the center of the cell by forming cytoplasmic clusters [62]. It is believed that the subcellular localization and distribution of the cytoplasmic chemoreceptor arrays are associated with the life cycle of bacteria [22]. Our results show that MCP<sub>514</sub> localizes cell poles. Although both CheW<sub>1</sub> and CheW<sub>2</sub> interact with MCP<sub>514</sub>, respectively, (Figure 5), the cellular localization of MCP<sub>514</sub> is independent of CheW (Figure 6), which is consistent with the previous results obtained from *E. coli*, in which trimers of homodimers of MCPs form clusters of MCPs and in turn recruit CheA/CheW to assemble MCP-CheW-CheA ternary complexes [52,54]. In combination with the previous studies on other cytoplasmic MCPs [22,62], our results could support that this TM-lacking chemoreceptor, MCP<sub>514</sub>, localizes the cell poles through interacting with other transmembrane chemoreceptors, although the experimental evidence may be required to demonstrate the interaction of MCP<sub>514</sub> with other MCPs.

According to the previous studies on Tsr and Tar of *E. coli*, the hairpin (HP) subdomain of MCP is not only the region forming homodimeric MCP but also the contacting sites for the formation of mixed trimers as well as the assembly of MCP-CheW-CheA ternary complexes [51,55]. Five conserved amino acid residues in the two antiparallel helices of *E. coli* Tsr (Phe373, Asn381, Glu385, Arg388 and Val353) are important for the cluster formation and function of MCP [51]. Hydrophobic interactions between the helices contribute to the main trimer packing forces [55]. Five corresponding residues of MCP<sub>514</sub> conducted the single residue of the respective substitution. Phe328 of MCP<sub>514</sub> is in the key site of the helical structure of the HP subdomain. The replacement of Phe328 by the helix destroyer, proline, results in MCP<sub>514</sub> diffusing in the cytoplasm. Replacement of Phe328 by alanine does not affect both the cellular location and chemotactic function of MCP<sub>514</sub>. These results demonstrate that Phe328 is not the direct determinant to the chemotactic function of MCP<sub>514</sub>, but indirectly affects MCP<sub>514</sub> function through stabilizing the helical structure. Amongst the five tested MCP<sub>514</sub> variants, three variants have the full function of the wildtype, which is slightly different from the results of *E. coli* Tsr [51].

## 5. Conclusions

MCP<sub>514</sub> is localized at cell poles, although it lacks a transmembrane region. The cellular localization of MCP<sub>514</sub> is independent of the assembly of MCP-CheW-CheA ternary complex but dependent on the interaction with other MCPs through the hairpin (HP) subdomain. Compared with other MCPs, MCP<sub>514</sub> plays a superior role in maintaining the signaling efficiency of the whole chemoreceptor signaling team. The helical structure of the hairpin subdomain is the prerequisite of MCP<sub>514</sub> cellular localization and functioning. The molecular mechanism of MCP<sub>514</sub> interacting with other MCPs and functioning in the chemotaxis signaling is similar to that of *E. coli* MCPs, although the roles of some key residues of MCP<sub>514</sub> in the transducing signal are slightly different from those of *E. coli* Tsr.

**Supplementary Materials:** The following are available online at <https://www.mdpi.com/article/10.3390/microorganisms9091923/s1>, Figure S1: Construction procedure, screening and verification of *atu0514*-deficient mutants. Figure S2: Sequence alignment of three *A. fabrum* MCPs and two *E. coli* MCPs. Table S1: Bacterial strains and plasmids used in this study. Table S2: Primers used in this study

**Author Contributions:** Conceptualization, J.Y. and M.G. (Minliang Guo); data curation, J.Y. and Q.Z.; formal analysis, J.Y., M.G. (Miaomiao Gao), Q.Z., H.W., N.X. and M.G. (Minliang Guo); funding acquisition, M.G. (Minliang Guo); investigation, J.Y., M.G. (Miaomiao Gao) and Q.Z.; methodology, J.Y., H.W. and N.X.; project administration, M.G. (Minliang Guo); supervision, M.G. (Minliang Guo); writing—original draft, J.Y.; writing—review and editing, M.G. (Minliang Guo). All authors have read and agreed to the published version of the manuscript.

**Funding:** This work was funded by the National Natural Science Foundation of China (Grant No. 31870118, 21808196, 31170073).

**Institutional Review Board Statement:** Not applicable.

**Informed Consent Statement:** Not applicable.

**Data Availability Statement:** The data that support the findings of this study are available from the corresponding author upon reasonable request.

**Acknowledgments:** We thank Yan Lu (the testing and analysis center of Yangzhou University) for help with the confocal laser microscopy observation.

**Conflicts of Interest:** The authors declare no conflict of interest.

## References

1. Dogra, G.; Purschke, F.G.; Wagner, V.; Haslbeck, M.; Kriehuber, T.; Hughes, J.G.; Van Tassell, M.L.; Gilbert, C.; Niemeyer, M.; Ray, W.K.; et al. *Sinorhizobium meliloti* CheA complexed with CheS exhibits enhanced binding to CheY1, resulting in accelerated CheY1 dephosphorylation. *J. Bacteriol.* **2012**, *194*, 1075–1087. [[CrossRef](#)]
2. Sourjik, V.; Wingreen, N.S. Responding to chemical gradients: Bacterial chemotaxis. *Curr. Opin. Cell Biol.* **2012**, *24*, 262–268. [[CrossRef](#)] [[PubMed](#)]
3. Parkinson, J.S.; Hazelbauer, G.L.; Falke, J.J. Signaling and sensory adaptation in *Escherichia coli* chemoreceptors: 2015 update. *Trends Microbiol.* **2015**, *23*, 257–266. [[CrossRef](#)] [[PubMed](#)]
4. Hazelbauer, G.L.; Falke, J.J.; Parkinson, J.S. Bacterial chemoreceptors: High-performance signaling in networked arrays. *Trends Biochem. Sci.* **2008**, *33*, 9–19. [[CrossRef](#)] [[PubMed](#)]
5. Sourjik, V. Receptor clustering and signal processing in *E. coli* chemotaxis. *Trends Microbiol.* **2004**, *12*, 569–576. [[CrossRef](#)] [[PubMed](#)]
6. Wadhams, G.; Martin, A.C.; Porter, S.; Maddock, J.; Mantotta, J.; King, H.; Armitage, J. TlpC, a novel chemotaxis protein in *Rhodobacter sphaeroides*, localizes to a discrete region in the cytoplasm. *Mol. Microbiol.* **2003**, *46*, 1211–1221. [[CrossRef](#)] [[PubMed](#)]
7. Bi, S.; Lai, L. Bacterial chemoreceptors and chemoeffectors. *Cell. Mol. Life Sci.* **2015**, *72*, 691–708. [[CrossRef](#)]
8. Karmakar, R. State of the art of bacterial chemotaxis. *J. Basic Microbiol.* **2021**, *61*, 366–379. [[CrossRef](#)]
9. Ortega, A.; Zhulin, I.; Krell, T. Sensory repertoire of bacterial chemoreceptors. *Microbiol. Mol. Biol. Rev.* **2017**, *81*, e00033-17. [[CrossRef](#)]
10. Sampedro, I.; Parales, R.E.; Krell, T.; Hill, J.E. *Pseudomonas* chemotaxis. *FEMS Microbiol. Rev.* **2015**, *39*, 17–46. [[CrossRef](#)]
11. Gavira, J.A.; Gumerov, V.M.; Rico-Jimenez, M.; Petukh, M.; Upadhyay, A.A.; Ortega, A.; Matilla, M.A.; Zhulin, I.B.; Krell, T. How bacterial chemoreceptors evolve novel ligand specificities. *mBio* **2020**, *11*, e03066-19. [[CrossRef](#)] [[PubMed](#)]
12. Guo, M.; Huang, Z.; Yang, J. Is there any crosstalk between the chemotaxis and virulence induction signaling in *Agrobacterium tumefaciens*? *Biotechnol. Adv.* **2017**, *35*, 505–511. [[CrossRef](#)]
13. Adadevoh, J.S.; Triolo, S.; Ramsburg, C.A.; Ford, R.M. Chemotaxis increases the residence time of bacteria in granular media containing distributed contaminant sources. *Environ. Sci. Technol.* **2016**, *50*, 181–187. [[CrossRef](#)] [[PubMed](#)]
14. Ud-Din, A.; Khan, M.F.; Roujeinikova, A. Broad specificity of amino acid chemoreceptor CtaA of *Pseudomonas fluorescens* is afforded by plasticity of its amphipathic ligand-binding pocket. *Mol. Plant Microbe Interact.* **2020**, *33*, 612–623. [[CrossRef](#)]
15. Yang, W.; Briegel, A. Diversity of bacterial chemosensory arrays. *Trends Microbiol.* **2020**, *28*, 68–80. [[CrossRef](#)] [[PubMed](#)]
16. Zhulin, I. The superfamily of chemotaxis transducers: From physiology to genomics and back. *Adv. Microb. Physiol.* **2001**, *45*, 157–198. [[CrossRef](#)]
17. Lacal, J.; Garcia-Fontana, C.; Munoz-Martinez, F.; Ramos, J.L.; Krell, T. Sensing of environmental signals: Classification of chemoreceptors according to the size of their ligand binding regions. *Environ. Microbiol.* **2010**, *12*, 2873–2884. [[CrossRef](#)]
18. Schultz, J.; Milpetz, F.; Bork, P.; Ponting, C. SMART, a simple modular architecture research tool: Identification of signaling domains. *Proc. Natl. Acad. Sci. USA* **1998**, *95*, 5857–5864. [[CrossRef](#)]

19. Xie, Z.; Ulrich, L.E.; Zhulin, I.B.; Alexandre, G. PAS domain containing chemoreceptor couples dynamic changes in metabolism with chemotaxis. *Proc. Natl. Acad. Sci. USA* **2010**, *107*, 2235–2240. [[CrossRef](#)]
20. Schweinitzer, T.; Mizote, T.; Ishikawa, N.; Dudnik, A.; Inatsu, S.; Schreiber, S.; Suerbaum, S.; Aizawa, S.; Josenhans, C. Functional characterization and mutagenesis of the proposed behavioral sensor TlpD of *Helicobacter pylori*. *J. Bacteriol.* **2008**, *190*, 3244–3255. [[CrossRef](#)] [[PubMed](#)]
21. Hou, S.; Larsen, R.; Boudko, D.; Riley, C.; Karatan, E.; Zimmer, M.; Ordal, G.; Alam, M. Myoglobin-like aerotaxis transducers in archaea and bacteria. *Nature* **2000**, *403*, 540–544. [[CrossRef](#)]
22. Collins, K.D.; Lacal, J.; Ottemann, K.M. Internal sense of direction: Sensing and signaling from cytoplasmic chemoreceptors. *Microbiol. Mol. Biol. Rev.* **2014**, *78*, 672–684. [[CrossRef](#)]
23. Escobar, M.A.; Dandekar, A.M. *Agrobacterium tumefaciens* as an agent of disease. *Trends Plant Sci.* **2003**, *8*, 380–386. [[CrossRef](#)]
24. Pitzschke, A.; Hirt, H. New insights into an old story: *Agrobacterium*-induced tumour formation in plants by plant transformation. *EMBO J.* **2010**, *29*, 1021–1032. [[CrossRef](#)]
25. Guo, M.; Bian, X.; Wu, X.; Wu, M. *Agrobacterium*-mediated genetic transformation: History and progress. In *Genetic Transformation*; Alvarez, M., Ed.; InTech: Rijeka, Croatia, 2011.
26. Kado, C.I. Historical account on gaining insights on the mechanism of crown gall tumorigenesis induced by *Agrobacterium tumefaciens*. *Front. Microbiol.* **2014**, *5*, 340. [[CrossRef](#)]
27. Yuan, Z.C.; Williams, M. A really useful pathogen, *Agrobacterium tumefaciens*. *Plant Cell* **2012**, *24*, tpc.112.tt1012. [[CrossRef](#)] [[PubMed](#)]
28. Hawes, M.; Smith, L. Requirement for chemotaxis in pathogenicity of *Agrobacterium tumefaciens* on roots of soil-grown pea plants. *J. Bacteriol.* **1989**, *171*, 5668–5671. [[CrossRef](#)] [[PubMed](#)]
29. Ashby, A.; Watson, M.; Loake, G.; Shaw, C. Ti plasmid-specified chemotaxis of *Agrobacterium tumefaciens* C58C1 toward vir-inducing phenolic compounds and soluble factors from monocotyledonous and dicotyledonous plants. *J. Bacteriol.* **1988**, *170*, 4181–4187. [[CrossRef](#)] [[PubMed](#)]
30. Loake, G.; Ashby, A.; Shaw, C. Attraction of *Agrobacterium tumefaciens* C58C1 towards sugars involves a highly sensitive chemotaxis system. *J. Gen. Microbiol.* **1988**, *134*, 1427–1432. [[CrossRef](#)]
31. Parke, D.; Ornston, L.; Nester, E. Chemotaxis to plant phenolic inducers of virulence genes is constitutively expressed in the absence of the Ti plasmid in *Agrobacterium tumefaciens*. *J. Bacteriol.* **1987**, *169*, 5336–5338. [[CrossRef](#)]
32. Winans, S. Two-way chemical signaling in *Agrobacterium*-plant interactions. *Microbiol. Rev.* **1992**, *56*, 12–31. [[CrossRef](#)] [[PubMed](#)]
33. Wood, D.W.; Setubal, J.C.; Kaul, R.; Monks, D.E.; Kitajima, J.P.; Okura, V.K.; Zhou, Y.; Chen, L.; Wood, G.E.; Almeida, N.F., Jr.; et al. The genome of the natural genetic engineer *Agrobacterium tumefaciens* C58. *Science* **2001**, *294*, 2317–2323. [[CrossRef](#)] [[PubMed](#)]
34. Goodner, B.; Hinkle, G.; Gattung, S.; Miller, N.; Blanchard, M.; Qurollo, B.; Goldman, B.S.; Cao, Y.; Askenazi, M.; Halling, C.; et al. Genome sequence of the plant pathogen and biotechnology agent *Agrobacterium tumefaciens* C58. *Science* **2001**, *294*, 2323–2328. [[CrossRef](#)]
35. Sambrook, J.; Russel, D. *Molecular Cloning: A Laboratory Manual*, 3rd ed.; Cold Spring Harbor Laboratory: Cold Spring Harbor, NY, USA, 2001.
36. Cangelosi, G.A.; Best, E.A.; Martinetti, G.; Nester, E.W. Genetic analysis of *Agrobacterium*. *Methods Enzymol.* **1991**, *204*, 384–397. [[CrossRef](#)] [[PubMed](#)]
37. Gelvin, S.B. *Agrobacterium* virulence gene induction. *Methods Mol. Biol.* **2006**, *343*, 77–84. [[CrossRef](#)]
38. Guo, M.; Hou, Q.; Hew, C.L.; Pan, S.Q. *Agrobacterium* VirD2-binding protein is involved in tumorigenesis and redundantly encoded in conjugative transfer gene clusters. *Mol. Plant Microbe Interact.* **2007**, *20*, 1201–1212. [[CrossRef](#)]
39. Guo, M.L.; Zhu, Q.; Gao, D.K. Development and optimization of method for generating unmarked *A. tumefaciens* mutants. *Prog. Biochem. Biophys.* **2009**, *36*, 556–565. [[CrossRef](#)]
40. Huang, Z.; Zhou, Q.; Sun, P.; Yang, J.; Guo, M. Two *Agrobacterium tumefaciens* CheW proteins are incorporated into one chemosensory pathway with different efficiencies. *Mol. Plant Microbe Interact.* **2018**, *31*, 460–470. [[CrossRef](#)]
41. Higuchi, R. Using PCR to engineer DNA. In *PCR Technology*; Palgrave Macmillan: London, UK, 1989; pp. 61–70.
42. Adler, J. A method for measuring chemotaxis and use of the method to determine optimum conditions for chemotaxis by *Escherichia coli*. *Microbiology* **1973**, *74*, 77–91. [[CrossRef](#)]
43. Merritt, P.M.; Danhorn, T.; Fuqua, C. Motility and chemotaxis in *Agrobacterium tumefaciens* surface attachment and biofilm formation. *J. Bacteriol.* **2007**, *189*, 8005–8014. [[CrossRef](#)]
44. Miller, J. *Experiments in Molecular Genetics*; Cold Spring Harbor Laboratory: Cold Spring Harbor, NY, USA, 1972; Volume 172.
45. Alexander, R.; Zhulin, I. Evolutionary genomics reveals conserved structural determinants of signaling and adaptation in microbial chemoreceptors. *Proc. Natl. Acad. Sci. USA* **2007**, *104*, 2885–2890. [[CrossRef](#)]
46. Hirokawa, T.; Boon-Chieng, S.; Mitaku, S. SOSUI: Classification and secondary structure prediction system for membrane proteins. *Bioinformatics* **1998**, *14*, 378–379. [[CrossRef](#)]
47. Juretić, D.; Zoranić, L.; Zucić, D. Basic charge clusters and predictions of membrane protein topology. *J. Chem. Inf. Comput. Sci.* **2002**, *42*, 620–632. [[CrossRef](#)]
48. Greenfield, D.; McEvoy, A.L.; Shroff, H.; Crooks, G.E.; Wingreen, N.S.; Betzig, E.; Liphardt, J. Self-organization of the *Escherichia coli* chemotaxis network imaged with super-resolution light microscopy. *PLoS Biol.* **2009**, *7*, e1000137. [[CrossRef](#)] [[PubMed](#)]

49. Zhou, Q. Functional Identification of Methyl Accepting Chemotaxis Protein Encoded by Gene *atu0514* Located in the Chemotaxis Operon of *Agrobacterium tumefaciens*. Master's Thesis, Yangzhou University, Yangzhou, China, 2020.
50. Kim, K.K.; Yokota, H.; Sangjin, K. Four-helical-bundle structure of the cytoplasmic domain of a serine chemotaxis receptor. *Nature* **1999**, *400*, 787–792. [[CrossRef](#)] [[PubMed](#)]
51. Ames, P.; Studdert, C.; Reiser, R.; Parkinson, J. Collaborative signaling by mixed chemoreceptor teams in *Escherichia coli*. *Proc. Natl. Acad. Sci. USA* **2002**, *99*, 7060–7065. [[CrossRef](#)] [[PubMed](#)]
52. Studdert, C.; Parkinson, J. Crosslinking snapshots of bacterial chemoreceptor squads. *Proc. Natl. Acad. Sci. USA* **2004**, *101*, 2117–2122. [[CrossRef](#)] [[PubMed](#)]
53. Studdert, C.A.; Parkinson, J.S. Insights into the organization and dynamics of bacterial chemoreceptor clusters through in vivo crosslinking studies. *Proc. Natl. Acad. Sci. USA* **2005**, *102*, 15623–15628. [[CrossRef](#)]
54. Li, M.; Khursigara, C.M.; Subramaniam, S.; Hazelbauer, G.L. Chemotaxis kinase CheA is activated by three neighbouring chemoreceptor dimers as effectively as by receptor clusters. *Mol. Microbiol.* **2011**, *79*, 677–685. [[CrossRef](#)]
55. Gosink, K.K.; Zhao, Y.; Parkinson, J.S. Mutational analysis of N381, a key trimer contact residue in Tsr, the *Escherichia coli* serine chemoreceptor. *J. Bacteriol.* **2011**, *193*, 6452–6460. [[CrossRef](#)]
56. Wright, E.; Deakin, W.; Shaw, C. A chemotaxis cluster from *Agrobacterium tumefaciens*. *Gene* **1998**, *220*, 83–89. [[CrossRef](#)]
57. McCullen, C.A.; Binns, A.N. *Agrobacterium tumefaciens* and plant cell interactions and activities required for interkingdom macromolecular transfer. *Annu. Rev. Cell Dev. Biol.* **2006**, *22*, 101–127. [[CrossRef](#)]
58. Gelvin, S.B. Traversing the cell: *Agrobacterium* T-DNA's journey to the host genome. *Front. Plant Sci.* **2012**, *3*, 52. [[CrossRef](#)] [[PubMed](#)]
59. Pitzschke, A. *Agrobacterium* infection and plant defense—Transformation success hangs by a thread. *Front. Plant Sci.* **2013**, *4*, 519. [[CrossRef](#)] [[PubMed](#)]
60. Szurmant, H.; Ordal, G.W. Diversity in chemotaxis mechanisms among the bacteria and archaea. *Microbiol. Mol. Biol. Rev.* **2004**, *68*, 301–319. [[CrossRef](#)] [[PubMed](#)]
61. Meier, V.M.; Scharf, B.E. Cellular localization of predicted transmembrane and soluble chemoreceptors in *Sinorhizobium meliloti*. *J. Bacteriol.* **2009**, *191*, 5724–5733. [[CrossRef](#)]
62. Briegel, A.; Ladinsky, M.S.; Oikonomou, C.; Jones, C.W.; Harris, M.J.; Fowler, D.J.; Chang, Y.W.; Thompson, L.K.; Armitage, J.P.; Jensen, G.J. Structure of bacterial cytoplasmic chemoreceptor arrays and implications for chemotactic signaling. *Elife* **2014**, *3*, e02151. [[CrossRef](#)]